CMB anomalies and the effects of local features of the inflaton potential

Alexander Gallego Cadavid[1,5,7], Antonio Enea Romano[1,2,6,7], Stefano Gariazzo[2,3,4]

[1] *Yukawa Institute for Theoretical Physics, Kyoto University, Japan*

[2] *Department of Physics, University of Torino,*

Via P. Giuria 1, I–10125 Torino, Italy

[3] *INFN, Sezione di Torino, Via P. Giuria 1, I–10125 Torino, Italy*

[4] *Instituto de Física Corpuscular (CSIC-Universitat de València), Paterna (Valencia), Spain*

[5] *ICRANet, Piazza della Repubblica 10, I–65122 Pescara*

[6] *King's College London, Strand, London, WC2R 2LS, United Kingdom*

[7] *Instituto de Fisica, Universidad de Antioquia, A.A.1226, Medellin, Colombia*

arXiv:1612.03490v1 [astro-ph.CO] 11 Dec 2016

Abstract

Recent analysis of the WMAP and Planck data have shown the presence of a dip and a bump in the spectrum of primordial perturbations at the scales $k = 0.002$ Mpc^{-1} and $k = 0.0035$ Mpc^{-1} respectively. We analyze for the first time the effects a local feature in the inflaton potential to explain the observed deviations from scale invariance in the primordial spectrum. We perform a best fit analysis of the cosmic microwave background (CMB) radiation temperature and polarization data. The effects of the features can improve the agreement with observational data respect to the featureless model. The best fit local feature affects the primordial curvature spectrum mainly in the region of the bump, leaving the spectrum unaffected on other scales.

I. INTRODUCTION

There are important observational motivations to study modifications of the inflaton potential, like the observed deviations of the spectrum of primordial curvature perturbations from a from a power law spectrum [1–17]. In Refs. [1–13] the authors study the effects of analizing the cosmic microwave background (CMB) radiation using a free function for the spectrum of primordial scalar perturbations, i.e., they do not consider the usual power law spectrum predicted by most of the simplest inflationary models [14, 15, 18]. For example, the primordial spectrum can be parametrized with wavelets [4, 5], linear interpolation [6–8], interpolating spline functions [11–13], among other methods [1, 16].

Some interesting evidence of these deviations were given in [1, 16] where it was used a method based on a piecewise cubic Hermite interpolating polynomial (PCHIP) for the primordial power spectrum. This analysis showed that the spectrum of primordial perturbations can be approximated with a power law in the range of values $0.007\text{Mpc}^{-1} < k < 0.2\text{Mpc}^{-1}$ while in the range $0.001\text{Mpc}^{-1} < k < 0.0035\text{Mpc}^{-1}$ there are a dip and a bump at $k = 0.002$ Mpc^{-1} and $k = 0.0035$ Mpc^{-1}, with a statistical significance of about 2σ and 1σ, respectively. Similar results were reported in several other analyses [1–3, 14, 19–30] using different techniques and both the WMAP [31] and Planck [32, 33] measurements. In this paper we study how local features of the inflaton potential can model this type of local glitches of the spectrum of primordial curvature perturbations. We also study the effects of these features on the primordial tensorial perturbation spectrum.

Features of the inflaton potential can affect the evolution of primordial curvature perturbations [1, 34–51] and consequently generate a variation in the amplitude of the spectrum and bispectrum [34–43]. This can provide a better fit of the observational data in the regions where the spectrum shows some deviations a power law [1–3, 37, 38, 40–43, 48, 49, 52–54]. In this paper we perform a best fit analysis of the cosmic microwave background (CMB) radiation temperature and polarization data and we study the effects of a local feature of the inflation potential which affects the primordial curvature spectrum in the region of the bump.

II. LOCAL FEATURES

We consider a single scalar field minimally coupled to gravity with a standard kinetic term according to the action

$$S = \int d^4x\sqrt{-g}\left[\frac{1}{2}M_{Pl}^2 R - \frac{1}{2}g^{\mu\nu}\partial_\mu\phi\partial_\nu\phi - V(\phi)\right], \tag{1}$$

where $M_{Pl} = (8\pi G)^{-1/2}$ is the reduced Planck mass and $g_{\mu\nu}$ is the flat $FLRW$ metric. The Friedmann equation and the equation of motion of the inflaton are obtained from the variation of the action with respect to the metric and the scalar field respectively

$$H^2 \equiv \left(\frac{\dot{a}}{a}\right)^2 = \frac{1}{3M_{Pl}^2}\left(\frac{1}{2}\dot{\phi}^2 + V(\phi)\right), \tag{2}$$

$$\ddot{\phi} + 3H\dot{\phi} + \partial_\phi V = 0, \tag{3}$$

where H is the Hubble parameter, and dots and ∂_ϕ denote derivatives with respect to time and scalar field respectively. The slow-roll parameters are defined

$$\epsilon \equiv -\frac{\dot{H}}{H^2} \quad , \quad \eta \equiv \frac{\dot{\epsilon}}{\epsilon H}. \tag{4}$$

We consider a potential energy given by [36]

$$V(\phi) \;=\; V_0(\phi) + V_F(\phi)\,, \tag{5}$$

$$V_F(\phi) \;=\; \lambda e^{-(\frac{\phi-\phi_0}{\sigma})^2}\,, \tag{6}$$

where $V_0(\phi)$ is the featureless potential and V_F corresponds to a step symmetrically dumped by an even power negative exponential factor. In this paper we will consider the case of a quadratic inflaton potential

$$V_0(\phi) = \frac{1}{2}m^2\phi^2\,. \tag{7}$$

This type of modification of the slow-roll potential is called local feature (LF) [36] which differs from the branch feature (BF) [35, 36] since the potential is symmetric with respect to the location of the feature and it is only affected in a limited range of the scalar field value. Due to this the spectrum and bispectrum are only modified in a narrow range of scales, in contrast to the BF in which there are differences in the power spectrum between large and small scale which are absent in the case of LF. In this paper we use the local type effect of these features to model phenomenologically local glitches of the primordial scalar spectrum on the scales

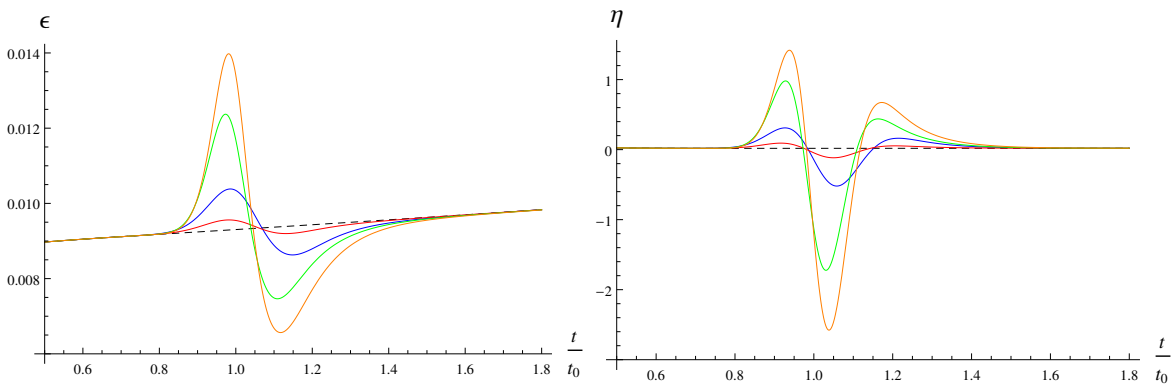

Figure 1: The numerically computed slow-roll parameters ϵ and η around the feature time t_0 for $\lambda = -4 \times 10^{-12}, \sigma = 0.05$, and $k_0 = 1.2 \times 10^{-3}$ (blue), $\lambda = -10^{-12}, \sigma = 0.05$, and $k_0 = 1.3 \times 10^{-3}$ (red), $\lambda = -10^{-11}, \sigma = 0.04$, and $k_0 = 1.3 \times 10^{-3}$ (green), and $\lambda = -1.5 \times 10^{-11}, \sigma = 0.04$, and $k_0 = 1.2 \times 10^{-3}$ (orange). The dashed lines correspond to the featureless slow roll parameters.

$k = 0.002\text{Mpc}^{-1}$ and $k = 0.0035\text{Mpc}^{-1}$ [1], and to study their effects on the primordial tensor spectrum, without affecting other scales.

The effects of the feature on the slow-roll parameters are shown in Fig 1, where we can see that there are oscillations of the slow-roll parameters around the feature time t_0, defined as $\phi_0 = \phi(t_0)$ [36]. The magnitude of the potential modification is controlled by the parameter λ, as its effect is such that larger value of λ give larger values of the slow-roll parameters. The size of the range of field values where the potential is affected by the feature is determined by the parameter σ and the slow-roll parameters are smaller for larger σ. We define k_0 as the scale exiting the horizon at the feature time t_0, $k_0 = -1/\tau_0$, where τ_0 is the value of conformal time corresponding to t_0. Oscillations occur around k_0, and their location can be controlled by changing ϕ_0. We adopt a system of units in which $c = \hbar = M_{Pl} = 1$.

III. SPECTRUM OF CURVATURE TENSOR PERTURBATIONS

In order to study the curvature perturbations we expand perturbatively the action with respect to the background $FLRW$ solution. The second order action for scalar perturbations in the comoving gauge takes the form [55]

$$S_2 = \int dt d^3x \left[a^3 \epsilon \dot{\zeta}^2 - a\epsilon(\partial\zeta)^2 \right] . \tag{8}$$

The equation for curvature perturbations ζ obtained from the Lagrange equations is

$$\frac{\partial}{\partial t}\left(a^3 \epsilon \frac{\partial \zeta}{\partial t} \right) - a\epsilon\delta^{ij}\frac{\partial^2\zeta}{\partial x^i \partial x^j} = 0. \tag{9}$$

Taking the Fourier transform and using conformal time $d\tau \equiv dt/a$ we get

$$\zeta_k'' + 2\frac{z'}{z}\zeta_k' + k^2\zeta_k = 0, \tag{10}$$

where k is the comoving wave number, $z \equiv a\sqrt{2\epsilon}$, and primes denote a derivative with respect to the conformal time. The two-point function of curvature perturbations is

$$\left\langle \hat{\zeta}(\vec{k}_1, t)\hat{\zeta}(\vec{k}_2, t)\right\rangle \equiv (2\pi)^3 \frac{2\pi^2}{k^3} P_\zeta(k)\delta^{(3)}(\vec{k}_1 + \vec{k}_2)\,, \tag{11}$$

where the power spectrum of curvature perturbations is defined as

$$P_\zeta(k) \equiv \frac{k^3}{2\pi^2}|\zeta_k|^2\,. \tag{12}$$

The effects of the features on the primordial scalar spectrum are plotted in Fig. 2 for different values of the parameters λ, σ, and k_0 [36]. The spectrum of primordial curvature perturbations has oscillations around k_0, whose amplitude is larger for larger λ since the latter controls the magnitude of the potential modification. The amplitude of the spectrum oscillations is larger for smaller σ, because in this case the change in the potential is more abrupt and consequently the slow-roll parameters are larger.

The equation for tensor perturbations can be derived in a way similar to the case of scalar perturbations, giving

$$h_k'' + 2\frac{a'}{a}h_k' + k^2 h_k = 0\,, \tag{13}$$

where again k is the comoving wave number. The power spectrum of tensor perturbations is obtained from the two-point function as

$$P_h(k) \equiv \frac{2k^3}{\pi^2}|h_k|^2\,, \tag{14}$$

from which the tensor-to-scalar ratio can be defined as the ratio between the spectrum of tensor and scalar perturbations as

$$r \equiv \frac{P_h}{P_\zeta}\,. \tag{15}$$

The effects of the features on the primordial tensor spectrum are plotted in Fig. 3 for different values of the parameters λ, σ, and k_0. These effects are not very significant and in fact the observational data analysis we will present in the rest of the paper confirms that local features affect mainly the curvature spectrum.

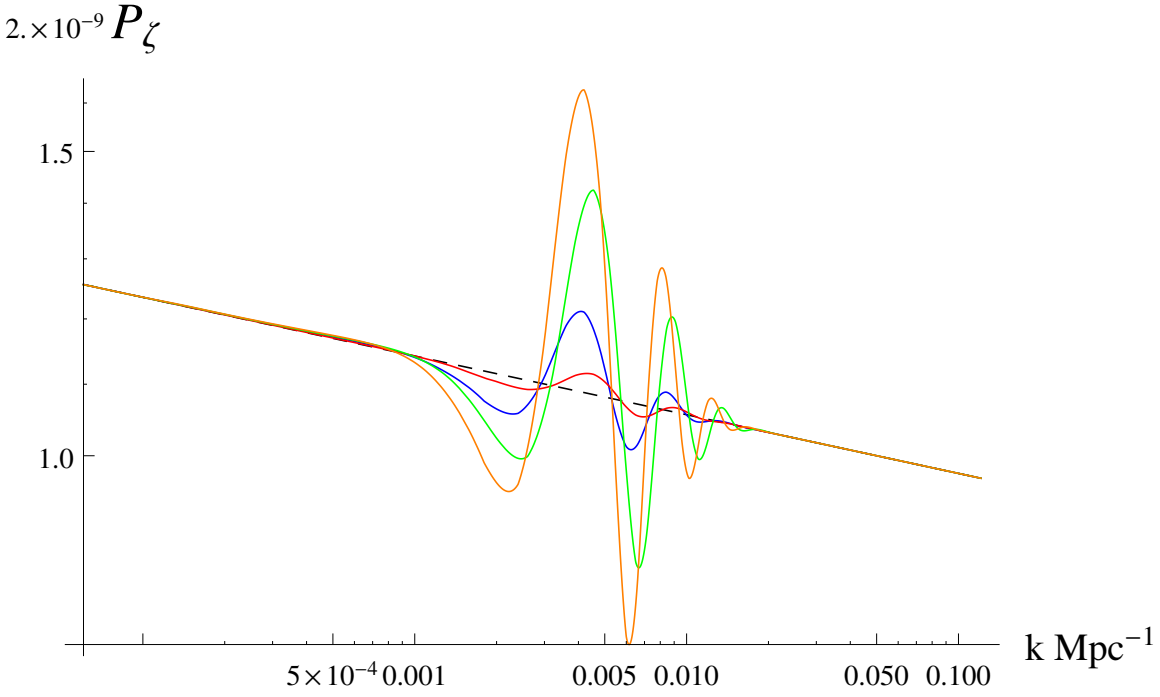

Figure 2: The power spectrum of primordial curvature perturbations P_ζ is plotted for $\lambda = -4 \times 10^{-12}, \sigma = 0.05$, and $k_0 = 1.2 \times 10^{-3}$ (blue), $\lambda = -10^{-12}, \sigma = 0.05$, and $k_0 = 1.3 \times 10^{-3}$ (red), $\lambda = -10^{-11}, \sigma = 0.04$, and $k_0 = 1.3 \times 10^{-3}$ (green), and $\lambda = -1.5 \times 10^{-11}, \sigma = 0.04$, and $k_0 = 1.2 \times 10^{-3}$ (orange). The dashed lines correspond to the featureless spectrum.

IV. EFFECTS OF LOCAL FEATURES ON THE CMB SPECTRUM

In Figs. 4 and 5 are shown the effects of local features on the temperature (TT) and B-mode polarization (BB) CMB spectra. Since we are considering a feature of local type, as theoretically expected, the spectrum is not affected on scales sufficiently far from k_0. Branch features [36] could on the contrary also introduce a step in the power spectrum, modifying it also on scales far from k_0, and for this reason LF are more appropriate to model local deviations of the spectrum.

The main effects produced by the LF appear between $\ell = 10$ and $\ell = 100$ in the TT spectrum. They correspond to the wiggles of the primordial scalar fluctuations shown in Fig. 2. The class of LF we consider allows to fit the small bump at $\ell \simeq 40$ better than the dip at $\ell \simeq 20$ in the CMB spectrum. The impact of the LF on the BB spectrum is much smaller, since, as discussed previously, the effect of the feature on the primordial tensorial perturbations spectrum is negligible.

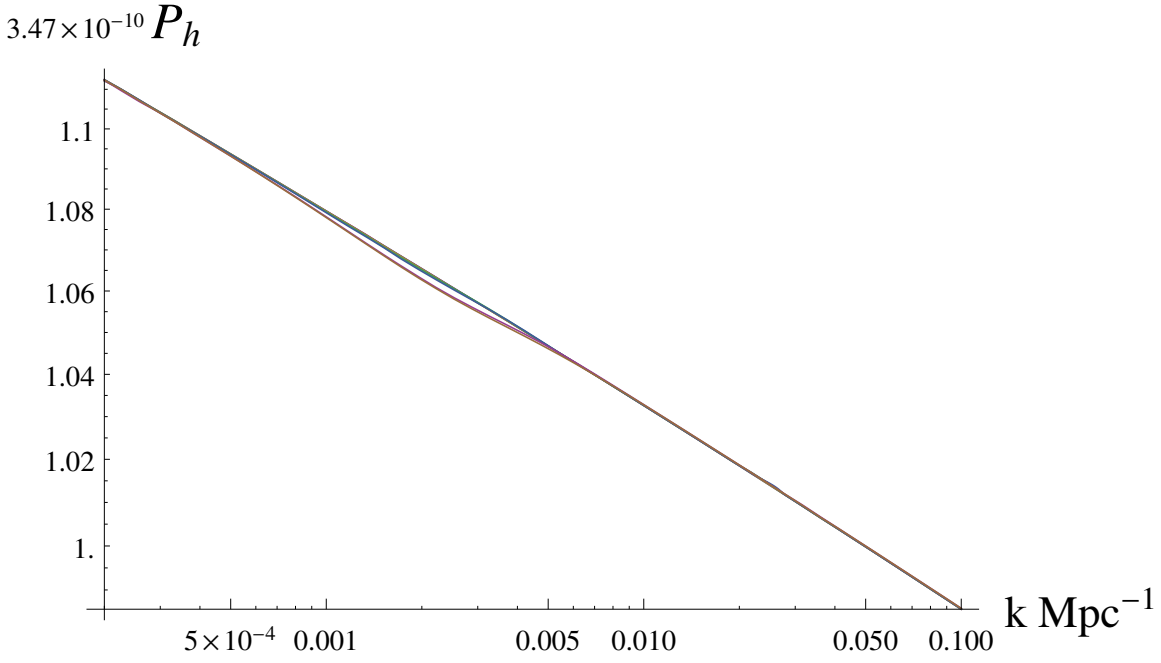

Figure 3: The power spectrum of primordial tensor perturbations P_h is plotted for $\lambda = -4\times10^{-12}, \sigma = 0.05$, and $k_0 = 1.2 \times 10^{-3}$ (blue), $\lambda = -10^{-12}, \sigma = 0.05$, and $k_0 = 1.3 \times 10^{-3}$ (red), $\lambda = -10^{-11}, \sigma = 0.04$, and $k_0 = 1.3 \times 10^{-3}$ (green), and $\lambda = -1.5 \times 10^{-11}, \sigma = 0.04$, and $k_0 = 1.2 \times -3$ (orange). The dashed lines correspond to the featureless spectrum. As it can be seen the effects of the different features on the spectrum P_h are rather small and the spectra of the models with features are difficult to distinguish from the featureless model spectrum.

A. The observational data analysis method

To study the effects produced by local features on the CMB spectrum, we modified the Boltzmann code `CAMB` [57] that computes the theoretical spectra and the corresponding Markov Chain Monte Carlo (MCMC) code `CosmoMC` [58] in order to use a non-standard power spectrum for the primordial curvature perturbations perturbations.

As a base model we considered the standard parameterization of the ΛCDM model for the evolution of the universe, that includes four parameters: the current energy density of baryons and of Cold Dark Matter (CDM) $\Omega_b h^2$ and $\Omega_c h^2$, the ratio between the sound horizon and the angular diameter distance at decoupling θ, and the optical depth to reionization τ.

The parameterization of the primordial power spectra is modified to take into account the presence of the local feature. To see the effects of the feature, we compare the results obtained in the featureless model with the ones obtained when a local feature is added. The comparison

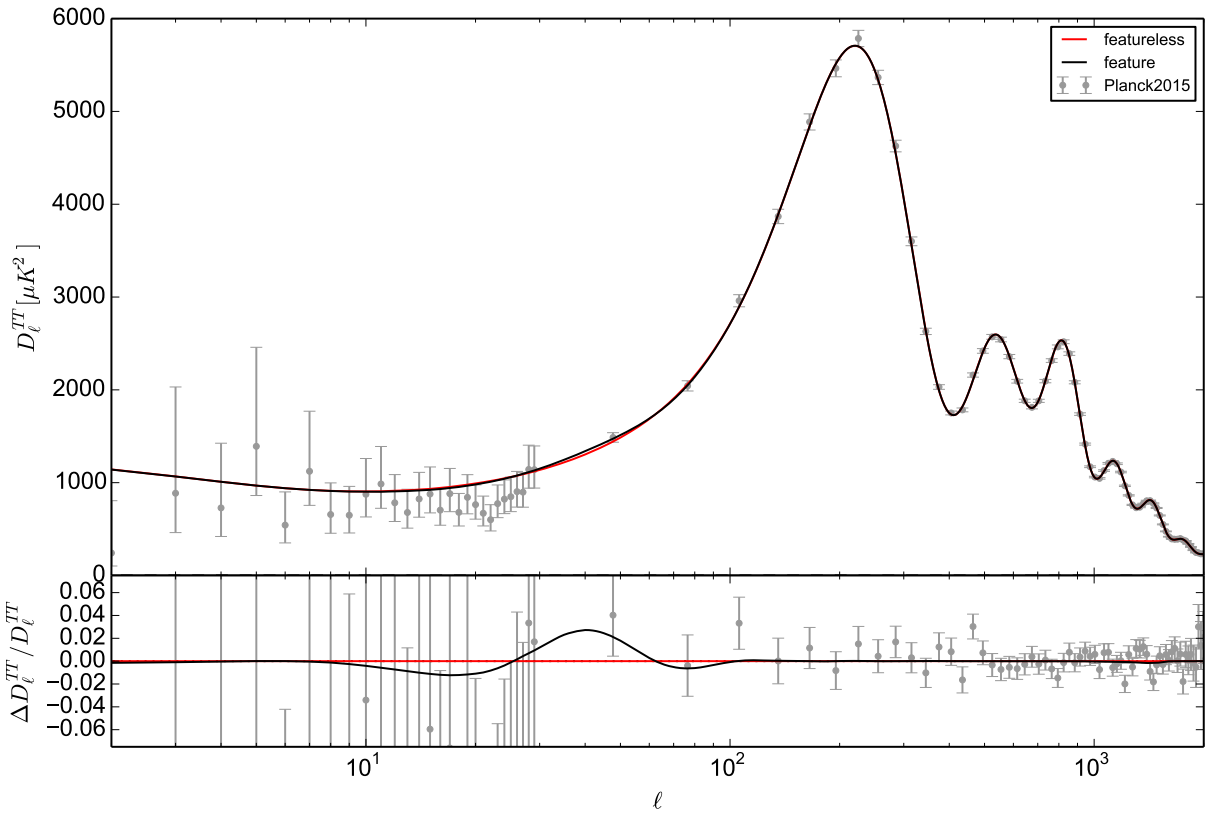

Figure 4: The $D_l^{TT} = \ell(\ell+1)C_\ell^{TT}/(2\pi)$ spectrum in units of μK^2 is plotted as a function of the multipole l. We compare the best-fit obtained using the inflationary model without feature (red line) to the one obtained introducing the local feature (black line). In the lower panel we plot the relative difference with respect to the featureless case. The data points are from the 2015 Planck release [33]. The cosmological parameters used to compute the two spectra are reported in Tab. I.

of the effects of LF of different inflationary potentials is left for future studies.

The data sets that we use to test the LF are taken from the last release from the Planck Collaboration [33] for the temperature and E-mode polarization modes. We consider the full temperature power spectrum at multipoles $2 \leq \ell \leq 2500$ ("Planck TT" hereafter) and the polarization power spectra in the range $2 \leq \ell \leq 29$ ("lowP"). Since the polarization spectra at high multipoles are still under discussion and some residual systematics were detected by the Planck Collaboration [59, 60], we do not include the full polarization spectra obtained by Planck. Moreover, we include the Bicep2/Keck BB mode data combined with the polarized dust emission Planck data [61]. We call this set of data BKP. The full set of data we analyze is then "Planck TT+lowP+BKP".

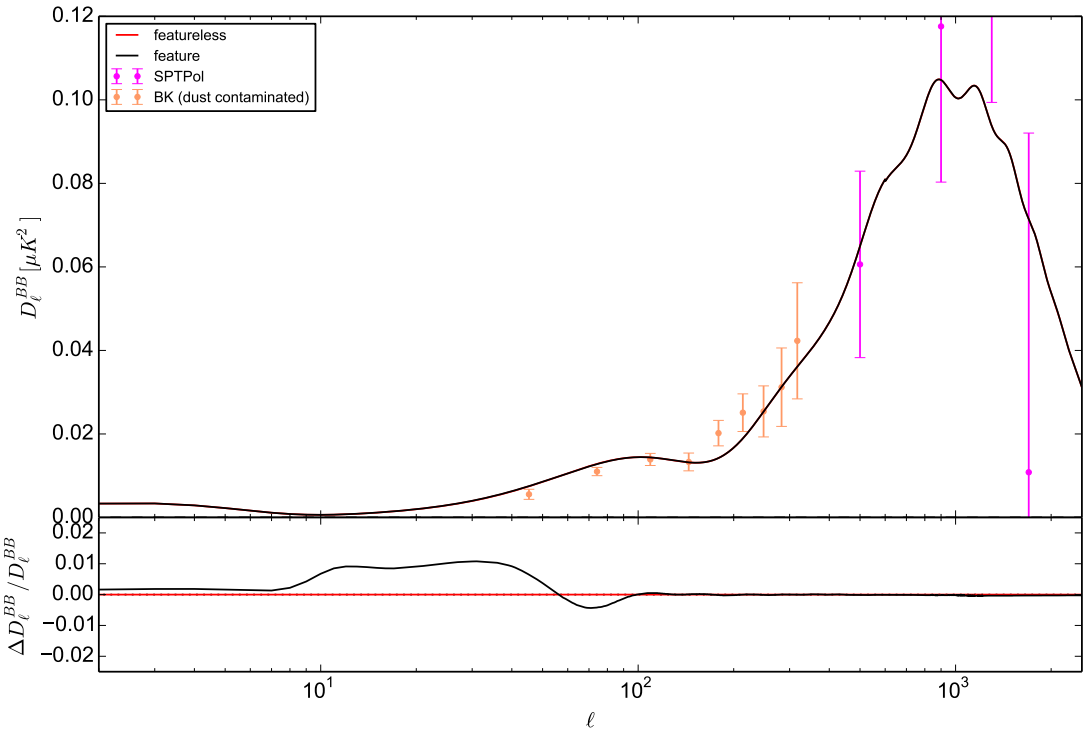

Figure 5: The $D_l^{BB} = \ell(\ell+1)C_\ell^{BB}/(2\pi)$ spectrum is plotted according to the same units and conventions as in Fig. 4. The purple data points are the lensing B-modes measurements obtained by SPTPol [56].

V. RESULTS

The results of the data fitting analysis are reported in Tab. I and in Figs. 7-10.

In Tab. I we show the best-fit values written inside brackets and the 1σ constraints of the parameters. Comparing the results obtained with and without feature we can see that the presence of the LF has no impact on the background cosmological parameters. This is clear from the marginalized 1D and 2D plots in Fig. 7. The effect of the feature is evident around the location of the bump of the CMB temperature spectrum (see Fig. 4), and it corresponds to an improvement of the total χ^2.

From the correlation plot between λ and k_0 we can see that the size of the feature can be larger if the feature is located at a smaller wavemode k_0. This is because the CMB temperature spectrum does not allow any wiggles above $\ell \simeq 60$, thus limiting the amplitude of the feature.

The constraints on the primordial scalar and tensor spectra are shown in Figs. 9 and 10, respectively. The 1, 2, and 3σ bands refer to the model with LF, and the solid black line

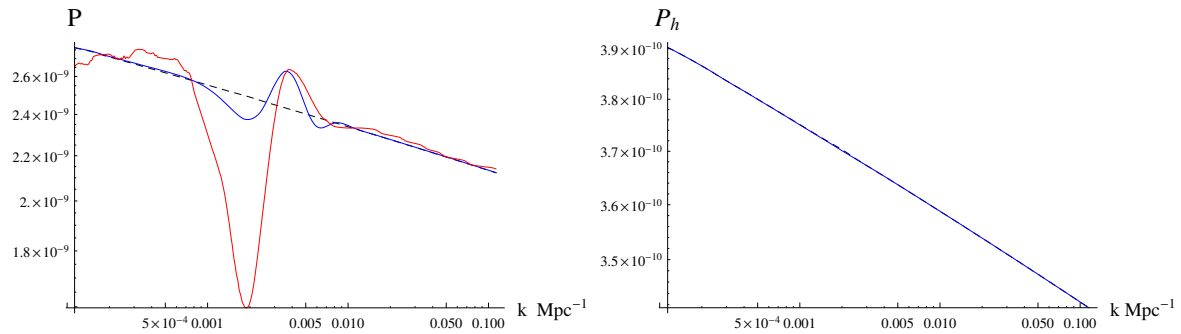

Figure 6: The numerically computed spectrum of the primordial curvature fluctuations P_ζ and of the tensor perturbations P_h are plotted for the best fit values in Tab. I: $\lambda = -1.12 \times 10^{-12}, \sigma = 0.053$, and $k_0 = 1.13 \times 10^{-3}$ (blue). On the left the red lines correspond to the best-fit reconstructed primordial power spectrum from Ref. [16]. The dashed lines correspond to the featureless spectrum.

Parameter	with feature	featureless
$10^2\omega_b$	2.203 ± 0.019	2.203 ± 0.019
ω_c	0.121 ± 0.001	0.121 ± 0.001
θ	1.0406 ± 0.0004	1.0406 ± 0.0004
τ	0.057 ± 0.015	0.059 ± 0.015
$\ln(10^{10} A_s)$	3.053 ± 0.031	3.054 ± 0.031
H_0	66.5 ± 0.5	66.5 ± 0.5
$-10^{12}\lambda$	$[0.05, 1.2)$ $\{1.12\}$	-
$10^2\sigma$	$5.3\,^{+1.3}_{-3.0}$	-
$10^3 k_0$	$[1.0, 1.3)$ $\{1.13\}$	-
χ^2	11342.0	11343.8

Table I: Constraints on the cosmological parameters and χ^2 for the model with and without feature. All the constraints are given at 1σ confidence level. The lower limits on the feature parameters correspond to the limits we used as a prior. The best fit are values inside curly brackets. The best fit χ^2 values are typically within $\Delta\chi^2 \sim 1$ of the true global best-fit value.

shows the corresponding best-fit spectrum, calculated marginalizing the entire set of primordial spectra obtained from the MCMC scan. From the figures can note that the effects of the feature are more important for the scalar spectrum while they are negligible for the tensor spectrum.

Further studies of the effects of local features on different inflation potentials are left for

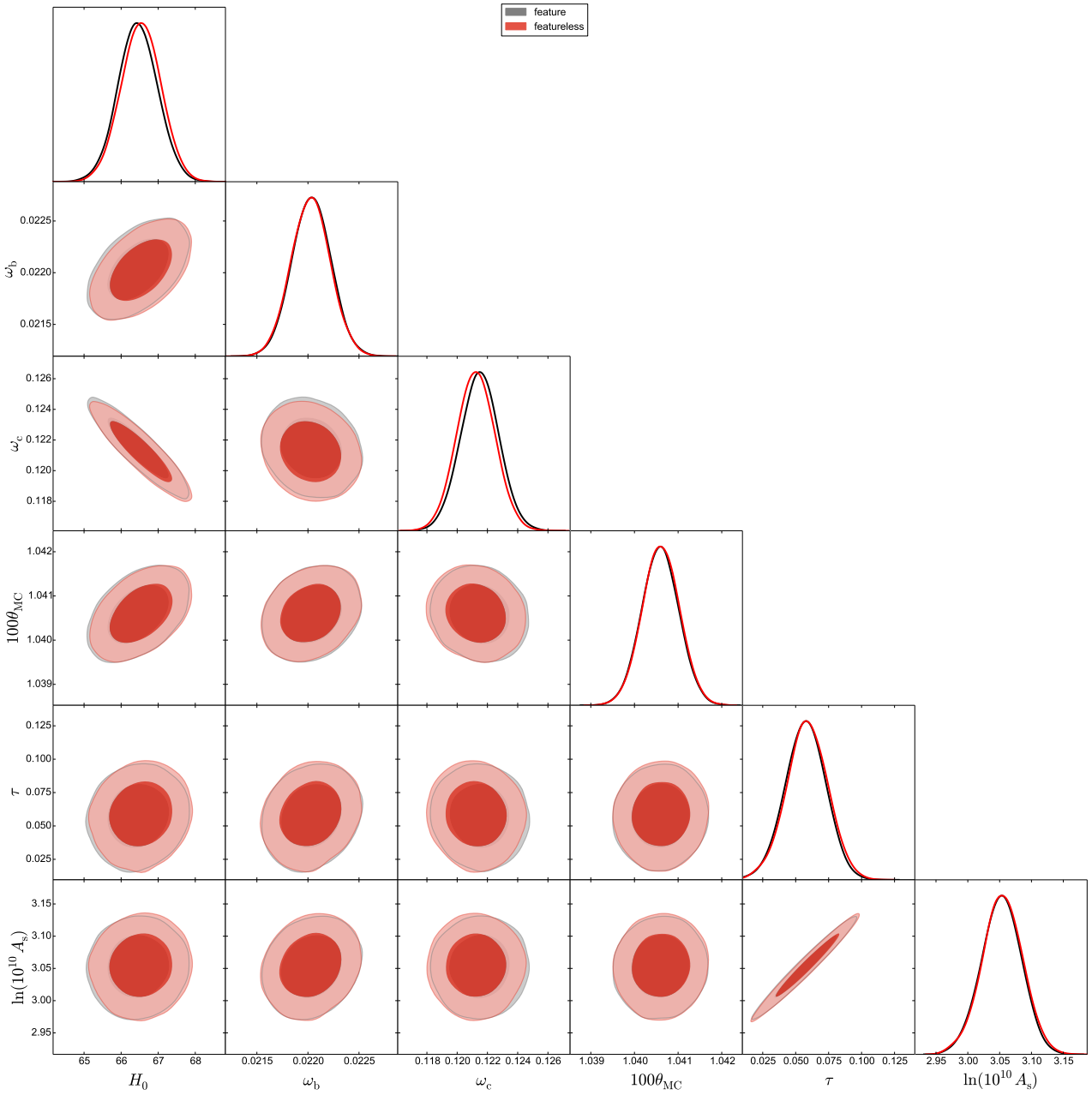

Figure 7: A comparison between the model with and without features is given for the parameters H_0, ω_b, ω_c, θ, τ and $\ln(10^{10}A_s)$. All the results are obtained considering the Planck+BKP data combination. As can be seen the effects of the feature on the estimation of these non inflationary cosmological parameters is negligible.

future analysis.

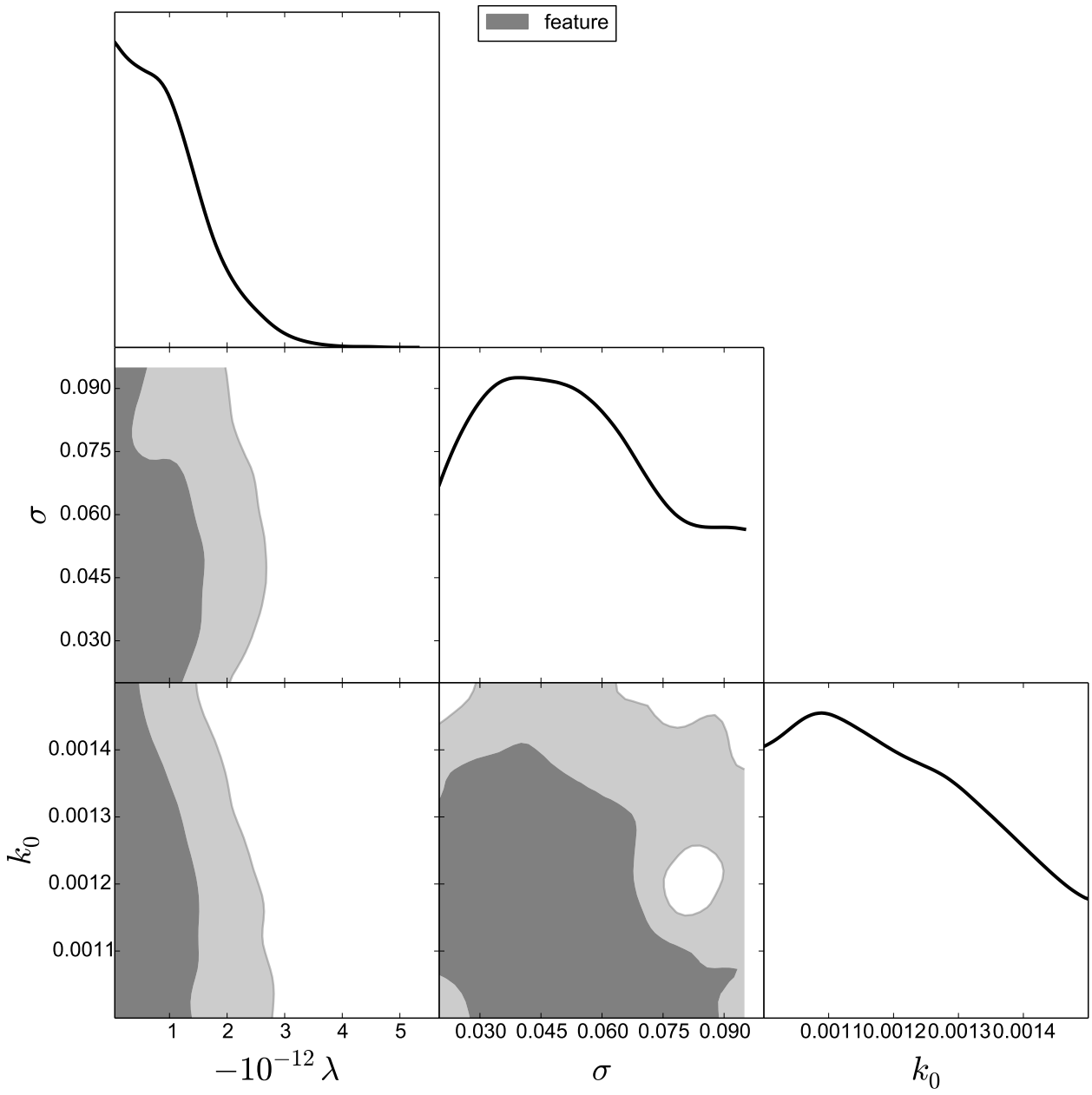

Figure 8: The results of the data fitting analysis for the parameters λ, σ and k_0 are shown for the model with local features.

VI. CONCLUSIONS

We have studied the effects of local features in the inflaton potential on the spectra of primordial curvature perturbations and their impact on the temperature anisotropies of the CMB. In order to study the effects on the CMB spectrum we have modified the `CAMB` and `CosmoMC` codes in order to use a non-standard power-law power spectrum for the primordial

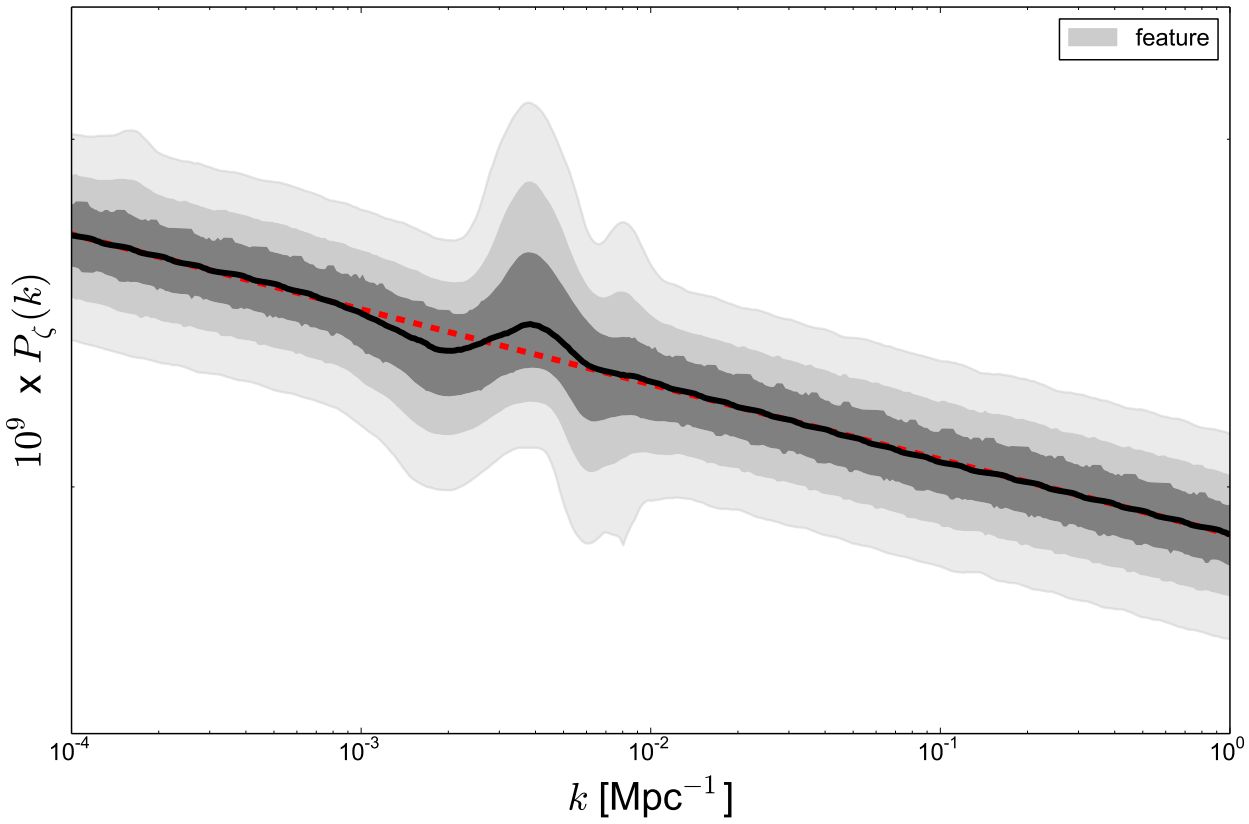

Figure 9: The 1, 2 and 3σ constraints obtained from observational data analysis are plotted for the primordial curvature perturbations spectrum for the model with local features. The spectrum for the featureless model is plotted with a red line.

perturbations, to take into account the presence of the local feature. We have performed a best fit analysis of CMB temperature and polarization data from Bicep2/Keck and Planck. We have found no significant effects on cosmological parameters related to the propagation of CMB photons after decoupling, while LF improve the fit of the CMB temperature and polarization data. We have also confirmed the theoretical expectation that local features do not affect the primordial power spectrum at scales far from the characteristic scale k_0, which leaves the horizon around the feature time.

In the future it will be interesting to analyze the effects of local features in order to explain other deviations of the CMB spectrum, such as for example the anomalies occurring around $l \approx 800$ [2]. It will also be important to study the effects of LF in inflationary models with different featureless V_0 potentials, and to compare them to the effects of branch features.

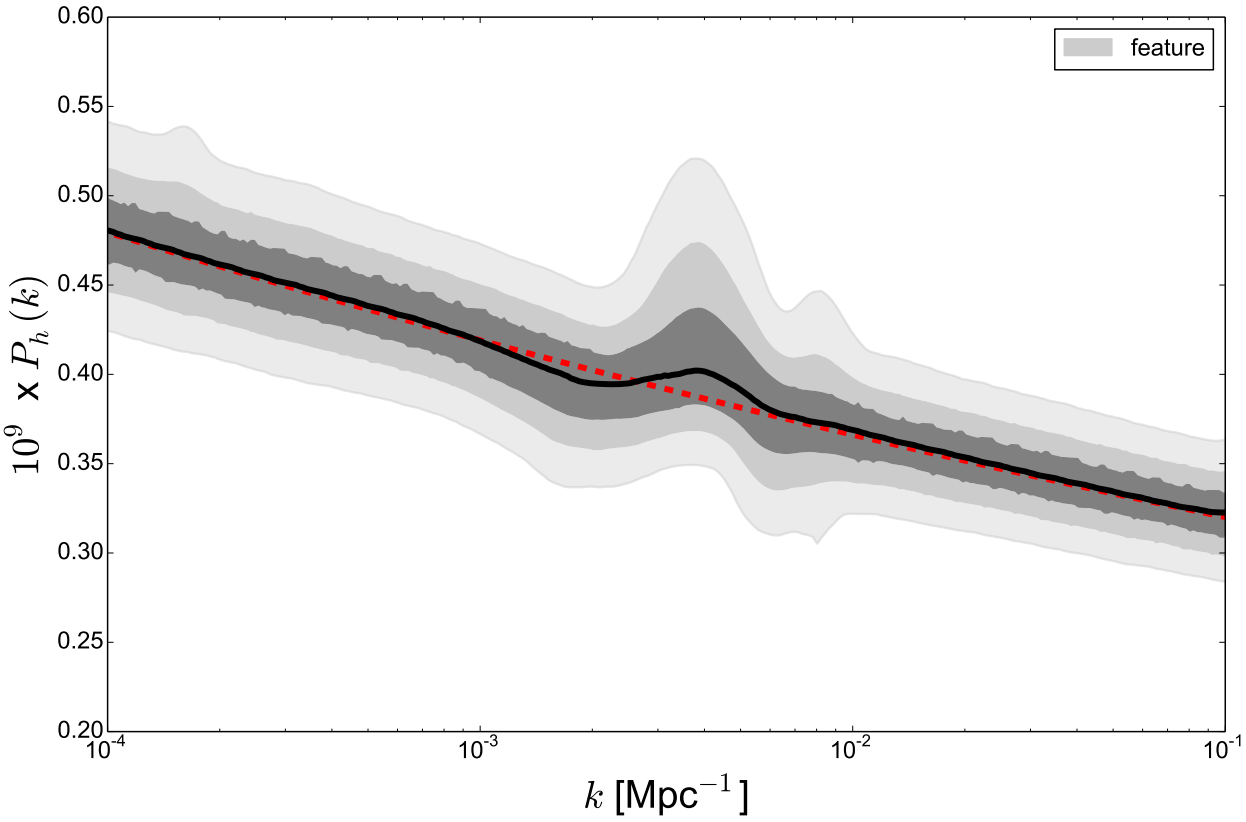

Figure 10: The 1, 2 and 3σ constraints obtained from observational data analysis are plotted for the primordial tensor perturbations power spectrum for the model with features. The spectrum for the featureless model is plotted with a red line.

Acknowledgments

This work was supported by the European Union (European Social Fund, ESF) and Greek national funds under the ARISTEIA II Action. Part of the work of S.G. was supported by the Theoretical Astroparticle Physics research Grant No. 2012CPPYP7 under the Program PRIN 2012 funded by the Ministero dell'Istruzione, Università e della Ricerca (MIUR), and in part is also supported by the Spanish grants FPA2014-58183-P, Multidark CSD2009-00064 and SEV-2014-0398 (MINECO), and PROMETEOII/2014/084 (Generalitat Valenciana). For part of the calculations we used the Cloud infrastructure of the Centro di Calcolo in the Torino section of INFN.

[1] S. Gariazzo, C. Giunti, and M. Laveder, JCAP **1504**, 023 (2015), arXiv:1412.7405.

[2] D. K. Hazra, A. Shafieloo, and T. Souradeep, JCAP **1411**, 011 (2014), arXiv:1406.4827.

[3] P. Hunt and S. Sarkar, JCAP **1401**, 025 (2014), arXiv:1308.2317.

[4] P. Mukherjee and Y. Wang, Astrophys. J. **593**, 38 (2003), arXiv:astro-ph/0301058.

[5] P. Mukherjee and Y. Wang, Astrophys. J. **599**, 1 (2003), arXiv:astro-ph/0303211.

[6] S. L. Bridle, A. M. Lewis, J. Weller, and G. Efstathiou, Mon. Not. Roy. Astron. Soc. **342**, L72 (2003), arXiv:astro-ph/0302306.

[7] D. K. Hazra, A. Shafieloo, and G. F. Smoot, JCAP **1312**, 035 (2013), arXiv:1310.3038.

[8] J. A. Vazquez, M. Bridges, Y.-Z. Ma, and M. P. Hobson, JCAP **1308**, 001 (2013), arXiv:1303.4014.

[9] S. Hannestad, Phys. Rev. **D63**, 043009 (2001), arXiv:astro-ph/0009296.

[10] M. Bridges, F. Feroz, M. P. Hobson, and A. N. Lasenby, Mon. Not. Roy. Astron. Soc. **400**, 1075 (2009), arXiv:0812.3541.

[11] D. K. Hazra, A. Shafieloo, G. F. Smoot, and A. A. Starobinsky, JCAP **1406**, 061 (2014), arXiv:1403.7786.

[12] C. Gauthier and M. Bucher, JCAP **1210**, 050 (2012), arXiv:1209.2147.

[13] R. de Putter, E. V. Linder, and A. Mishra, Phys. Rev. **D89**, 103502 (2014), arXiv:1401.7022.

[14] Planck Collaboration, P. Ade *et al.*, (2015), arXiv:1502.02114.

[15] Planck Collaboration, P. Ade *et al.*, (2013), arXiv:1303.5082.

[16] E. Di Valentino, S. Gariazzo, M. Gerbino, E. Giusarma, and O. Mena, Phys. Rev. **D93**, 083523 (2016), arXiv:1601.07557.

[17] M. Benetti and J. S. Alcaniz, Phys. Rev. **D94**, 023526 (2016), arXiv:1604.08156.

[18] J. Martin, C. Ringeval, and V. Vennin, (2013), arXiv:1303.3787.

[19] A. Shafieloo and T. Souradeep, Phys. Rev. **D70**, 043523 (2004), arXiv:astro-ph/0312174.

[20] G. Nicholson and C. R. Contaldi, JCAP **0907**, 011 (2009), arXiv:0903.1106.

[21] D. K. Hazra, A. Shafieloo, and T. Souradeep, Phys. Rev. **D87**, 123528 (2013), arXiv:1303.5336.

[22] G. Nicholson, C. R. Contaldi, and P. Paykari, JCAP **1001**, 016 (2010), arXiv:0909.5092.

[23] P. Hunt and S. Sarkar, (2015), arXiv:1510.03338.

[24] G. Goswami and J. Prasad, Phys. Rev. **D88**, 023522 (2013), arXiv:1303.4747.

[25] M. Matsumiya, M. Sasaki, and J. Yokoyama, Phys. Rev. **D65**, 083007 (2002), arXiv:astro-ph/0111549.

[26] M. Matsumiya, M. Sasaki, and J. Yokoyama, JCAP **0302**, 003 (2003), arXiv:astro-ph/0210365.

[27] N. Kogo, M. Matsumiya, M. Sasaki, and J. Yokoyama, Astrophys. J. **607**, 32 (2004), arXiv:astro-ph/0309662.

[28] N. Kogo, M. Sasaki, and J. Yokoyama, Prog. Theor. Phys. **114**, 555 (2005), arXiv:astro-ph/0504471.

[29] R. Nagata and J. Yokoyama, Phys. Rev. **D78**, 123002 (2008), arXiv:0809.4537.

[30] E. Di Valentino, S. Gariazzo, E. Giusarma, and O. Mena, Phys. Rev. **D91**, 123505 (2015), arXiv:1503.00911.

[31] WMAP, C. Bennett *et al.*, Astrophys.J.Suppl. **208**, 20 (2013), arXiv:1212.5225.

[32] Planck Collaboration, P. Ade *et al.*, (2013), arXiv:1303.5062.

[33] Planck, R. Adam *et al.*, (2015), arXiv:1502.01582.

[34] A. Gallego Cadavid, Primordial non-Gaussianities produced by features in the potential of single slow-roll inflationary models, Master's thesis, University of Antioquia, 2013, arXiv:1508.05684.

[35] A. G. Cadavid and A. E. Romano, Eur. Phys. J. **C75**, 589 (2015), arXiv:1404.2985.

[36] A. G. Cadavid, A. E. Romano, and S. Gariazzo, Eur. Phys. J. **C76**, 385 (2016), arXiv:1508.05687.

[37] H. Motohashi and W. Hu, (2015), arXiv:1503.04810.

[38] E. Komatsu *et al.*, (2009), arXiv:0902.4759.

[39] F. Arroja, A. E. Romano, and M. Sasaki, Phys.Rev. **D84**, 123503 (2011), arXiv:1106.5384.

[40] P. Adshead, C. Dvorkin, W. Hu, and E. A. Lim, Phys.Rev. **D85**, 023531 (2012), arXiv:1110.3050.

[41] X. Chen, R. Easther, and E. A. Lim, JCAP **0706**, 023 (2007), arXiv:astro-ph/0611645.

[42] X. Chen, R. Easther, and E. A. Lim, JCAP **0804**, 010 (2008), arXiv:0801.3295.

[43] J. A. Adams, B. Cresswell, and R. Easther, Phys.Rev. **D64**, 123514 (2001), arXiv:astro-ph/0102236.

[44] J. Chluba, J. Hamann, and S. P. Patil, Int. J. Mod. Phys. **D24**, 1530023 (2015), arXiv:1505.01834.

[45] X. Chen, JCAP **1201**, 038 (2012), arXiv:1104.1323.

[46] G. A. Palma, JCAP **1504**, 035 (2015), arXiv:1412.5615.

[47] A. A. Starobinsky, JETP Lett. **55**, 489 (1992).

[48] J. Hamann, L. Covi, A. Melchiorri, and A. Slosar, Phys.Rev. **D76**, 023503 (2007), arXiv:astro-ph/0701380.

[49] D. K. Hazra, M. Aich, R. K. Jain, L. Sriramkumar, and T. Souradeep, JCAP **1010**, 008 (2010), arXiv:1005.2175.

[50] D. K. Hazra, A. Shafieloo, G. F. Smoot, and A. A. Starobinsky, Phys.Rev.Lett. **113**, 071301

(2014), arXiv:1404.0360.

[51] D. K. Hazra, A. Shafieloo, G. F. Smoot, and A. A. Starobinsky, JCAP **1408**, 048 (2014), arXiv:1405.2012.

[52] M. Joy, V. Sahni, and A. A. Starobinsky, Phys.Rev. **D77**, 023514 (2008), arXiv:0711.1585.

[53] M. Joy, A. Shafieloo, V. Sahni, and A. A. Starobinsky, JCAP **0906**, 028 (2009), arXiv:0807.3334.

[54] M. J. Mortonson, C. Dvorkin, H. V. Peiris, and W. Hu, Phys.Rev. **D79**, 103519 (2009), arXiv:0903.4920.

[55] J. M. Maldacena, JHEP **0305**, 013 (2003), arXiv:astro-ph/0210603.

[56] R. Keisler *et al.*, Astrophys. J. **807**, 151 (2015), arXiv:1503.02315.

[57] A. Lewis, A. Challinor, and A. Lasenby, Astrophys. J. **538**, 473 (2000), arXiv:astro-ph/9911177.

[58] A. Lewis and S. Bridle, Phys. Rev. **D66**, 103511 (2002), arXiv:astro-ph/0205436.

[59] N. Aghanim *et al.*, Submitted to: Astron. Astrophys. (2015), 1507.02704.

[60] Planck, P. A. R. Ade *et al.*, (2015), arXiv:1502.01589.

[61] BICEP2 Collaboration, Planck Collaboration, P. Ade *et al.*, Phys.Rev.Lett. **114**, 101301 (2015), arXiv:1502.00612.